

Application of tumor-targeting peptide-decorated polypeptide nanoparticles with doxorubicin to treat osteosarcoma

Renna Qiu^{a*}, Denghua Sun^{b*}, Yuzhuo Bai^c, Jiannan Li^d and Lizhe Wang^e

^aDepartment of Physical Examination Center, China-Japan Union Hospital of Jilin University, Changchun, China; ^bDepartment of Breast Surgery, China-Japan Union Hospital of Jilin University, Changchun, China; ^cBreast and Thyroid Surgery, Affiliated Hospital of Changchun University of Traditional Chinese Medicine, Changchun, China; ^dDepartment of General Surgery, The Second Hospital of Jilin University, Changchun, China; ^eDepartment of Pediatric Oncology, The First Hospital of Jilin University, Changchun, China

ABSTRACT

Osteosarcoma is the most common primary malignant bone tumor in childhood and adolescence. Currently, surgery combined with chemotherapy is the main treatment for osteosarcoma. However, the long-term survival of patients with metastatic osteosarcoma is unsatisfactory. Therefore, new treatment methods to improve the prognosis of patients with osteosarcoma are required. The present study aimed to develop nanocarriers with both tumor targeting and reduction responsiveness abilities, and to improve the therapeutic effect and reduce toxicity by loading traditional small molecule anti-tumor drugs. The tumor targeting peptide-decorated, doxorubicin (DOX)-loaded mPEG-P(Phe-co-Cys) nanoparticles were developed successfully through the ring-opening polymerization of amino acids. The peptide VATANST (STP) can specifically bind with vimentin, which is highly expressed on the osteosarcoma cell surface, resulting in tumor targeting effects. The nanoparticle is core-shell structured to protect the loaded DOX during blood flow. The disulfide bonds within the nanoparticles are sensitive to the osteosarcoma microenvironment, which has high glutathione (GSH) levels. Under the enhanced permeability and retention and active tumor targeting effects, the STP-decorated DOX-loaded nanoparticles accumulated in tumor tissues. High GSH levels can rupture disulfide bonds, resulting in the controlled release of DOX, which will cause necrosis of tumor cells. The characteristics of the synthesized nanoparticles, DOX release profiles *in vitro* and *in vivo*, cytotoxicity analysis, animal study, and safety evaluation were performed. The nanoparticles could increase the tumor inhibition efficiency against osteosarcoma and reduce the side effects of DOX to major organs. The STP-decorated mPEG-P(Phe-co-Cys) nanoparticles might be a suitable drug delivery system for DOX to treat osteosarcoma.

ARTICLE HISTORY

Received 28 September 2020
Revised 22 November 2020
Accepted 23 November 2020

KEYWORDS



Doxorubicin; osteosarcoma; nanoparticle; tumor-targeting peptide; redox-responsive

Introduction

Osteosarcoma is the most common primary malignant bone tumor among children and adolescents (Marina et al., 2004). It has a high degree of malignancy and is prone to recurrence and metastasis (Harrison et al., 2018). Although surgery combined with chemotherapy has significantly improved the survival rate of patients with osteosarcoma, the long-term survival rate of patients with metastatic osteosarcoma is still only 15–20% (Qiu et al., 2019). Researchers have tried various methods to improve the efficiency of chemotherapy, including immunotherapy, targeted therapy, and other new treatment methods. However, there has been no major breakthrough in the treatment of osteosarcoma in the past 30 years (Botter et al., 2014; Eaton et al., 2020). Moreover, multi-drug resistance and severe side effects have limited the application and improvement of traditional chemotherapy for osteosarcoma (Yu et al., 2020). Therefore, researchers are trying to develop drug delivery systems to enhance the

effect of tumor treatment. Nano-drug delivery systems possess the advantages of good biocompatibility, stability, safety, controlled drug release, and easy structural modification (Li et al., 2018b; Feng et al., 2019; Su et al., 2020). These systems are expected to increase the targeted therapy ability and reduce toxicity by loading traditional small molecule anti-tumor drugs.

Doxorubicin (DOX) is the main chemotherapeutic drug used to treat osteosarcoma. However, chemotherapy resistance and cardiotoxicity limit its treatment efficacy (Ma et al., 2020; Ren & Su, 2020). To enhance the anti-tumor efficacy and reduce the side effects of DOX, we developed a kind of nanoparticles through the ring-opening polymerization of amino acids. The osteosarcoma microenvironment is significantly different from the surrounding normal tissues, and the surface of tumor cells expresses high levels of vimentin (Strouhalova et al., 2020; Wakhloo et al., 2020). The synthesized nanoparticles possess two internal disulfide bonds that

CONTACT Lizhe Wang  wanglizhe2005@163.com  Department of Pediatric Oncology, The First Hospital of Jilin University, Changchun 130021, China
*Renna Qiu and Denghua Sun contributed equally to this work.

© 2020 The Author(s). Published by Informa UK Limited, trading as Taylor & Francis Group.

This is an Open Access article distributed under the terms of the Creative Commons Attribution-NonCommercial License (<http://creativecommons.org/licenses/by-nc/4.0/>), which permits unrestricted non-commercial use, distribution, and reproduction in any medium, provided the original work is properly cited.

are sensitive to high levels of glutathione (GSH) in the osteosarcoma microenvironment. In addition, the nanoparticles were decorated with the peptide VATANST (STP), which can specifically bind with vimentin. DOX can be encapsulated within the nanoparticles in aqueous solution. Under passive and active tumor targeting effects, the STP-decorated poly-peptide nanoparticles loaded with DOX can accumulate in tumor tissues. The high levels of GSH then lead to the rupture of disulfide bonds (Wang et al., 2020b), resulting in the controlled release of DOX.

In this study, STP-decorated mPEG-P(Phe-co-Cys) copolymers were synthesized initially, followed by the encapsulation of DOX in aqueous solution. The DOX-loaded nanocarriers aimed to deliver DOX to tumor tissues efficiently and to control the release of DOX, thus increasing the chemotherapeutic effects of DOX toward osteosarcoma. The characteristics of the synthesized nanoparticles, the DOX release profiles *in vitro* and *in vivo*, cytotoxicity analysis, animal study, and safety evaluation were performed. The rationally designed structure of the STP-decorated mPEG-P(Phe-co-Cys) nanoparticles suggests that it might be a suitable drug delivery system for DOX to treat osteosarcoma.

Materials and methods

Materials

Polyethylene glycol monomethyl ether (mPEG), L-phenylalanine (L-Phe), L-cysteine (L-Cys), and deuterated trifluoroacetic acid (TFA-*d*) were purchased from Sigma-Aldrich (Shanghai, PR China). Dimethyl sulfoxide (DMSO), tetrahydrofuran (THF), N-hexane, toluene, N-hydroxysuccinimide (NHS), 1-ethyl-(3-dimethylaminopropyl) carbodiimide hydrochloride (EDC-HCl), and ether were bought from Beijing Chemical Works (Beijing, PR China). The peptide VATANST (STP), doxorubicin hydrochloride (DOX-HCl), and GSH were obtained from Gill Biochemical Co., Ltd. (Shanghai, PR China). Primary antibodies recognizing Ki-67 and caspase-3 were bought from Aladdin Reagent Co., Ltd. (Shanghai, PR China).

Preparation of mPEG-P(Phe-co-Cys) copolymers

The mPEG-P(Phe-co-Cys) copolymers were synthesized by ring-opening polymerization of L-Phe N-carboxy anhydride (NCA) and L-Cys NCA, based on the macroinitiation of mPEG-NH₂. In detail, mPEG-NH₂ was dissolved in toluene and then azeotroped at 120 °C to remove the remaining water in mPEG-NH₂. Then, dimethylformamide (DMF), L-Cys NCA, and L-Phe NCA were added into the above solution. The reaction was continued for 72 hours at 20 °C, and then the product obtained from the reaction was settled with ether, and dried under a vacuum at room temperature. The final product was mPEG-P(Phe-co-Cys) nanoparticles and was named as NPs in this study.

Preparation of STP-NPs

The *t*-BOC-NH-PEG-P(Phe-co-Cys) was prepared by ring-opening polymerization of L-Phe NCA and L-Cys NCA based on the macroinitiation of *t*-BOC-NH-PEG-NH₂. TFA-*d* was used to remove the *t*-BOC group and the product obtained from the reaction was settled with ether and dried under vacuum at room temperature to obtain the product NH₂-PEG-P(Phe-co-Cys). Then, NH₂-PEG-P(Phe-co-Cys) was reacted with maleimide, NHS, and EDC-HCl to obtain the product MI-PEG-P(Phe-co-Cys). Finally, the Michael addition reaction was applied to obtain STP-NPs (Li et al., 2018c).

Characterizations of NPs and STP-NPs

Proton nuclear magnetic resonance (¹H NMR) and Fourier-transform infrared (FT IR) spectroscopy were applied to analyze the characterizations of NPs and STP-NPs. ¹H NMR analysis of NPs and STP-NPs was performed using a 400 MHz Bruker spectrometer (Bruker, Billerica, MA) with CDCl₃ as the solvent. For FT IR analysis, the KBr tablet compression method was used to prepare the samples, and a Bio-Rad Win-IR instrument (Bio-Rad, Hercules, CA) was further applied. The sizes of NPs and STP-NPs were analyzed using dynamic light scattering (DLS) using a Wyatt QELS instrument (Wyatt Technology, Santa Barbara, CA). NPs and STP-NPs were dissolved in phosphate-buffered saline (PBS) solution or PBS containing 10.0 mM GSH, respectively, at a concentration of 0.2 mg/mL. The changes in the particle size of each kind of nanoparticles at pre-set time intervals in different solutions were recorded. The microscopic morphological characteristics of the nanoparticles were observed through JEM-1011 transmission electron microscopy (TEM; JEOL USA Inc., Peabody, MA) at a test voltage of 100 kV.

The biocompatibility of NPs and STP-NPs was assessed using the 3-(4,5-dimethylthiazol-2-yl)-2,5-diphenyltetrazolium bromide (MTT) method. Each well of a 96-well cell culture plate was added with high glucose (HG)-Dulbecco's modified Eagle's medium (DMEM) culture medium (200.0 μL, containing 6000 143B human osteosarcoma cells). After incubation for 24 hours at 37.0 °C and 5% CO₂, all the culture medium was removed. The HG-DMEM culture medium (180.0 μL) containing nanoparticles (0–40.0 mg L⁻¹) was added to each well and the culture was continued for 72 hours. Then, the MTT solution (20.0 μL, 5.0 mg L⁻¹) was added to each well and co-cultured for four hours. The absorbances of the solution in each well were determined by ultraviolet/visible (UV/vis) at 490 nm. The cell viability (%) was calculated using the following equation:

$$\text{Cell viability (\%)} = (\text{absorbance of sample} / \text{absorbance of control}) \times 100\% \quad (1)$$

Preparation of NPs/DOX and STP-NPs/DOX

NPs (300.0 mg) and DOX-HCl (106.2 mg) were dissolved in 18.0 mL and 2.0 mL of DMF, respectively. Then, the two solutions were mixed together, followed by the dropwise

addition of 18.0 mL distilled water and 2.0 mL PBS solution. The obtained solution was dialyzed for 24 hours to remove the remaining DMF and free DOX (F-DOX). Finally, the DOX-containing nanoparticles were obtained and named as NPs/DOX.

STP-NPs (301.0 mg) and DOX-HCl (107.9 mg) were dissolved in 18.0 mL and 2.0 mL of DMF, respectively. Similar procedures to those used for NPs/DOX were performed to obtain the DOX-containing STP-decorated nanoparticles, which were named as STP-NPs/DOX.

Characterizations of NPs/DOX and STP-NPs/DOX

The drug-loading content (DLC) and drug-loading efficiency (DLE) were calculated using the following equations:

$$\text{DLC (\%)} = \left(\frac{\text{the amount of drug in thenanoparticles}}{\text{total mass of thenanoparticles}} \right) \times 100\% \quad (2)$$

$$\text{DLE (\%)} = \left(\frac{\text{the amount of drug in thenanoparticles}}{\text{total amount of the drug}} \right) \times 100\% \quad (3)$$

The microscopic morphological characteristics and the size of NPs/DOX and STP-NPs/DOX were analyzed using TEM and DLS.

Drug release study

The *in vitro* DOX release of NPs/DOX and STP-NPs/DOX was assessed under the conditions of 37.0 °C and pH 7.4. NPs/DOX (1.0 mg) and STP-NPs/DOX (1.0 mg) were both dissolved in 10.0 mL PBS solution, with or without 10.0 mM GSH. The solutions were then dialyzed and the released DOX was analyzed by the UV/vis method at pre-set time intervals (0, 6, 12, 24, 48, 60, and 72 hours).

In vitro cellular uptake of DOX

The intracellular uptake study was analyzed using confocal laser scanning microscopy (CLSM) and flow cytometry (FCM) analysis. Each well of a six-well cell culture plate was added with HG-DMEM culture medium (2.0 mL, containing 2×10^5 143B human osteosarcoma cells). After incubation for 24 hours at 37.0 °C and 5% CO₂, all the culture medium was removed. HG-DMEM culture medium (2.0 mL) containing 10.0 mM GSH was added to each well and cultured for two hours. As a control group, HG-DMEM culture medium only was added to the control wells. Then, 10.0 mg L⁻¹ F-DOX, NPs/DOX, and STP-NPs/DOX were added to the above wells and the cells in culture medium were incubated for two hours. All the culture medium was then removed, and 4',6-diamidino-2-phenylindole (DAPI) and Alexa 488 were applied to stain the nuclei and F-actin, respectively. For FCM analysis, the procedures were similar with that of CLSM analysis. However, when all the culture medium was removed, the cells were treated with pancreatin, suspended in 1.0 mL of PBS solution, and centrifuged at 3000 rpm for four minutes. The supernatant was removed, the cell

suspension was further prepared, and 10,000 cells were collected for FCM detection.

In vitro cytotoxicity of NPs/DOX and STP-NPs/DOX

MTT analysis was used to assess the *in vitro* cytotoxicity of NPs/DOX and STP-NPs/DOX, toward 143B human osteosarcoma cells in the logarithmic growth phase. The cells in HG-DMEM culture medium containing 10.0 mM GSH was added to each well and cultured for two hours. As the control group, cells in HG-DMEM culture medium were added to the control wells. Then, F-DOX, NPs/DOX, and STP-NPs/DOX (0–100 mg L⁻¹) were added to each well and the cells were incubated for 72 hours for MTT analysis.

Animal study

Male BALB/c nude mice (5 weeks, 18.0–20.0 g) were purchased from Beijing Weitong Lihua Experimental Animal Technology Co., Ltd. (Beijing, PR China), and all the animal studies were performed in accordance with the protocol approved by the Animal Health and Use Committee of Jilin University. 143B human osteosarcoma cells (logarithmic growth phase, 1.0×10^8 /mL) were used to develop the osteosarcoma mice model. A 1.0 mL syringe was applied to penetrate the tibial plateau into the medullary cavity and 10.0 μL of the treated 143B cells were injected into the tibial medullary cavity.

Female Wistar rats (6 weeks, 180.0–200.0 g) were bought from the Animal Center of Jilin University for the *in vivo* pharmacokinetic study. The rats were randomly divided into three groups, with three animals in each group. Then, 10 mg/kg of F-DOX, NPs-DOX, or STP-NPs/DOX were administered via the tail vein. At pre-set time intervals (15 min and 30 min; and 1, 3, 6, 12, and 24 hours), blood samples were collected through the posterior eye vein. Blood samples were centrifuged and the supernatant was obtained. The amount of DOX was analyzed using high-performance liquid chromatography (HPLC) method and the mobile phase was methanol:KH₂PO₄ solution (2.7 g L⁻¹, prepared with ultrapure water, 70:30 (v/v)).

To assess the anti-tumor efficacy of F-DOX, NPs-DOX, and STP-NPs/DOX, the osteosarcoma mouse model was used. At the 10th day post the establishment of the osteosarcoma mouse model, the tumor volume was about 40 mm³. Then, 24 mice were randomly divided into four groups, including control, F-DOX, NPs-DOX, and STP-NPs/DOX groups. At the 10th, 15th, 20th, and 25th days post the establishment of the osteosarcoma mouse model, 0.2 mL PBS, F-DOX, NPs-DOX, or STP-NPs/DOX solutions (DOX, 5.0 mg/kg) were administered in each group via the tail vein. The body weight of each mouse was recorded and the tumor volume was also calculated using the following equation:

$$\text{Tumor volume (mm}^3\text{)} = \frac{4}{3} \pi \left[\frac{1}{4} (D_1 + D_2) \right] \quad (4)$$

where D_1 and D_2 represent the maximum diameter of the tumor around the patella and the maximum diameter of the tumor along the tibia, respectively. At the 30th day post

the establishment of the osteosarcoma mouse model, the mice were euthanized. The tumor, heart, liver, spleen, lung, and kidney tissues were collected. The organ coefficient was calculated using the following equation:

$$\text{Organ coefficient (\%)} = \frac{\text{the weight of organ/body weight}}{\text{total body weight}} \times 100\% \quad (5)$$

The tumor tissues and major organs were stored in paraformaldehyde solution (4%), sectioned at 5 μm , and stained using hematoxylin and eosin (H&E). For the tumor tissues, the relative necrotic area was analyzed using NIS-Elements imaging software (Nikon, Tokyo, Japan). The relative necrotic area was calculated using the following equation:

$$\text{Relative necrotic area (\%)} = \frac{\text{necrotic area within tumor tissue}}{\text{total area of tumor tissue}} \times 100\% \quad (6)$$

To further assess the anti-tumor efficacy in the different groups, the levels of Ki-67 and caspase-3 within tumor tissues were analyzed using immunofluorescence. Detailed procedures can be found in a previous study (Li et al., 2018a). CLSM and Image J software (NIH, Bethesda, MD) were applied to analyze the expression levels of Ki-67 and caspase-3 in the different groups.

Statistical analysis

All data are presented as the mean \pm standard deviation (SD) and analyzed using GraphPad Prism 7.0 software (GraphPad Inc., La Jolla, CA). Student's *t* test was used for the analysis. **p* < .05 was considered statistically significant, and ***p* < .01 and ****p* < .001 were considered as highly statistically significant.

Results and discussion

In this study, STP-decorated, DOX-loaded mPEG-P(Phe-co-Cys) nanoparticles were successfully developed. STP can specifically bind to vimentin, which is highly expressed on the cell surface of osteosarcoma, thus resulting in the tumor targeting effects of STP-NPs/DOX. The nanoparticles are core-shell structured, which can protect the loaded DOX during its passage through the blood flow. The disulfide bonds within the nanoparticles are sensitive to the osteosarcoma microenvironment, which has high levels of GSH. Under enhanced permeability and retention (EPR) (Yang et al., 2020) and active tumor targeting effects, STP-NPs/DOX can accumulate in tumor tissues. There are significant differences in GSH levels between tumor tissues and normal tissues *in vivo*. The concentration of GSH is 1.0–2.0 $\mu\text{mol/L}$ in plasma, 2.0–20.0 $\mu\text{mol/L}$ in normal tissues, and 2.0–10.0 mmol/L in tumor cells (Schafer & Buettner, 2001). The GSH concentration in tumor cells is more than 1000 times higher than that outside of tumor cells, and more than four times higher than that in normal cells. High levels of GSH can lead to the rupture of disulfide bonds (Wang et al., 2020b), leading to the controlled release of DOX, which will further result in tumor

cell necrosis. As a result, STP-NPs/DOX can release DOX efficiently within tumor tissues and are relatively stable in normal tissues. Similarly, under the *in vitro* environment which has high levels of GSH, the disulfide bonds of STP-NPs/DOX are ruptured and the loaded DOX can be released. Figure 1 illustrates the development of STP-NPs/DOX and its anti-tumor mechanisms.

NPs and STP-NPs/DOX were successfully developed in this study. According to the ^1H NMR analysis, the spectra at 3.8 ppm and 7.0 ppm indicated the proton of the methylene group in PEG and the proton of benzene ring in the L-Phe group (Figure 2(A)). Based on the element analysis, the proportions of C, H, N, and S in mPEG-P(Phe-co-Cys) copolymer were 53.03%, 8.49%, 1.84%, and 3.46%, respectively. There were four Cys and 12 Phe on each PEG chain, and the molecular weight of mPEG-P(Phe-co-Cys) copolymer was 7704 g mol^{-1} . In addition, there were specific signal peaks in the corresponding positions of PEG and polyphenylalanine groups that indicated the successful synthesis of STP-NPs (Figure 2(A)). Similarly, the proportions of C, H, N, and S in STP-mPEG-P(Phe-co-Cys) copolymer were 50.95%, 7.79%, 3.79%, and 6.75%, respectively. The molecular weight of STP-mPEG-P(Phe-co-Cys) copolymer was 8799 g mol^{-1} . The results of FT-IR further confirmed the successful preparation of STP-NPs (Figure 2(B)). The signal peaks at 1660 ($\text{V}_{\text{C}=\text{O}}$) and 1524 ($\text{V}_{\text{C}(\text{O})-\text{NH}}$) indicated the amides bonds.

The mPEG-P(Phe-co-Cys) copolymer self-assembled into spherical nanoparticles in aqueous solution with a diameter of 48.0 ± 11.4 nm (Figure 3(A)). DLS measurement of the particle size of the nanoparticles indicated that the diameter of the nanoparticles was 61.6 ± 34.8 nm (Figure 3(B)). Compared with the TEM results, the particle sizes the nanoparticles, as measured using DLS, were larger. This might have been caused by the dehydration and shrinkage of the nanoparticles during the preparation of the TEM samples. The STP-PEG-P(Phe-co-Cys) copolymer could also self-assemble into spherical nanoparticles with a diameter of 51.2 ± 15.2 nm in aqueous solution (Figure 3(C)). Based on the DLS analysis, the diameter of the nanoparticles was 61.0 ± 33.6 nm (Figure 3(D)). The particle size has a great influence on the distribution of nanocarriers in the body. Different tumor tissues have different requirements for particle size because of their different biological behaviors and permeability. It is generally accepted that the most suitable particle size for tumor treatment is 10–200 nm (Torchilin, 2007; Wang et al., 2011). The upper limit of the particle size to confirm the penetration into solid tumors is 400 nm, and when the diameter is less than 200 nm, it is more effective to achieve passive drug targeting via the EPR effect (Torchilin, 2011; Maeda et al., 2013). Particles smaller than 10 nm will be removed by glomerular filtration (Choi et al., 2007). In addition, the morphology of nanocarriers also plays an important role in the distribution of particles in the body, blood clearance, and cell internalization (Wang et al., 2011; Gu et al., 2015). Spherical particles are more likely to be endocytosed by tumor cells. The nanoparticles synthesized in the present study had a suitable size and morphology for use to carry drugs for anti-tumor research.

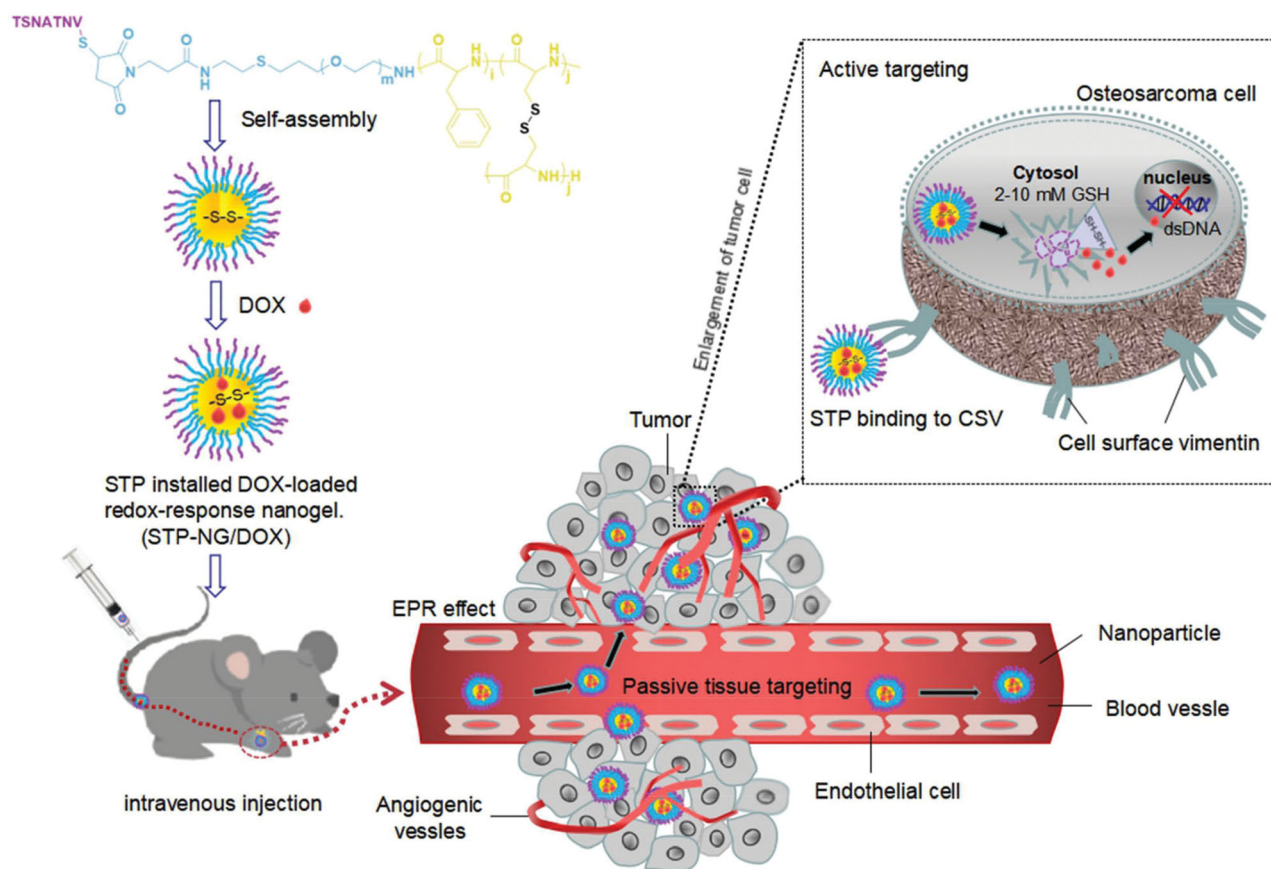


Figure 1. Illustration of STP-NPs/DOX development and its anti-tumor mechanisms.

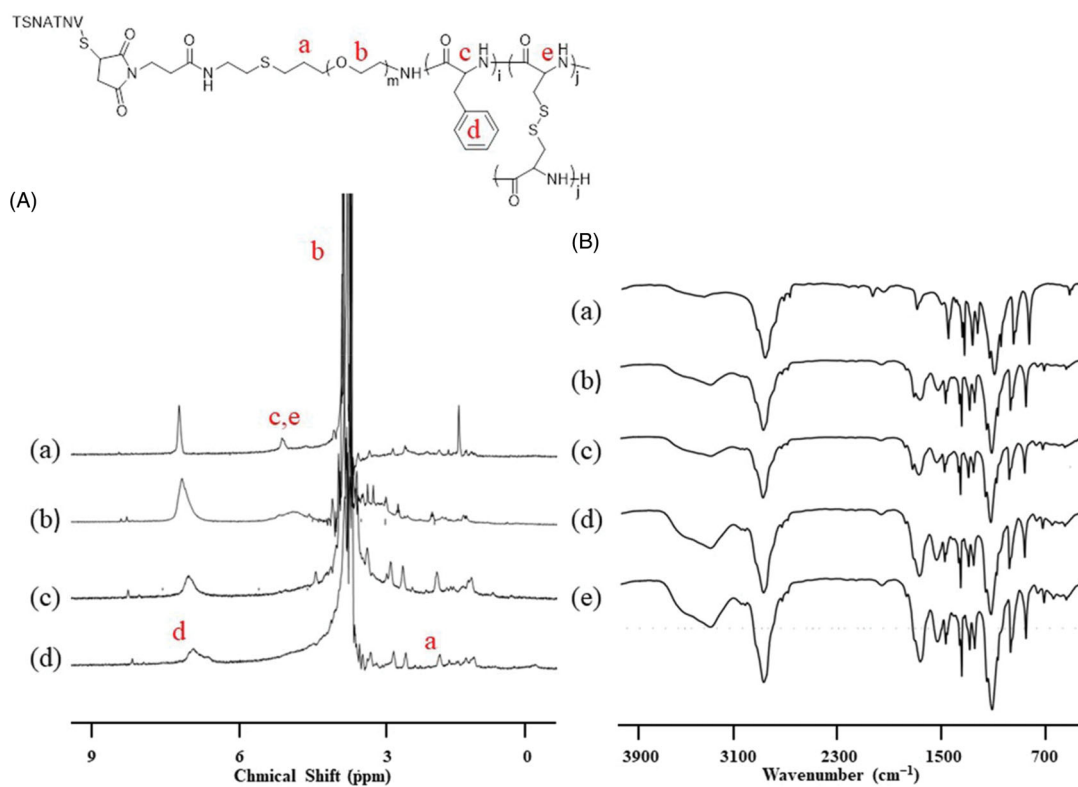


Figure 2. ^1H NMR and FT-IR analysis. (A) ^1H NMR spectra of (a) *t*-BOC-NH-PEG-P(Phe-co-Cys), (b) NH₂-PEG-P(Phe-co-Cys), (c) MI-PEG-P(Phe-co-Cys), and (d) STP-NPs. (B) FT-IR spectra of (a) *t*-BOC-NH-PEG-NH₂, (b) *t*-BOC-NH-PEG-P(Phe-co-Cys), (c) NH₂-PEG-P(Phe-co-Cys), (d) MI-PEG-P(Phe-co-Cys), and (e) STP-NPs.

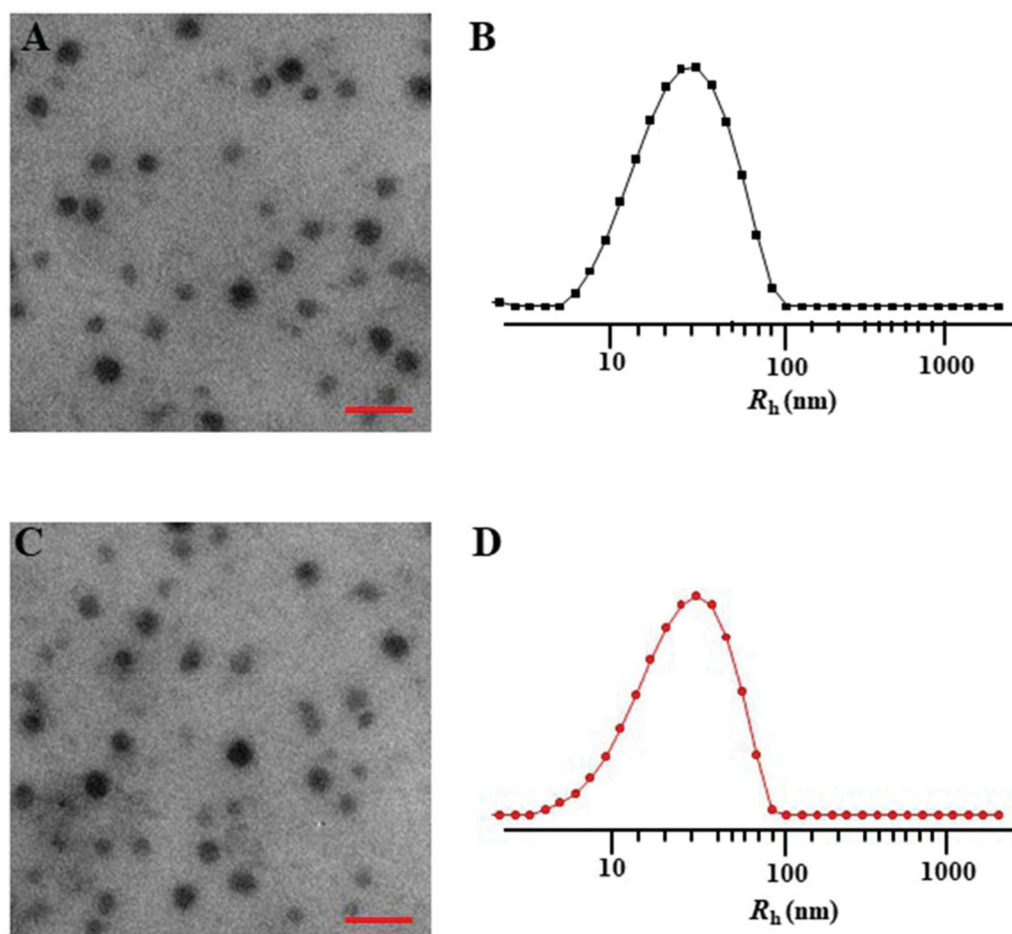


Figure 3. Typical TEM micrographs (A, C) and $R_{h,s}$ determined by DLS (B, D). NPs (A, B) and STP-NPs (C, D). Scale bar = 200 nm.

To assess the stability and reduction responsiveness of the two kinds of nanoparticles, we dispersed NPs and STP-NPs in PBS buffer solution, with or without 10.0 mM GSH. As a reducing agent, GSH is an important substance that maintains the redox state in the tumor microenvironment (Chen et al., 2020; Wang et al., 2020a). GSH can diffuse into the inner core of the nanoparticles and decompose the disulfide bond (–SS–) into two sulfhydryl groups (–SH), which will cause swelling of the nanoparticles and a change in particle size. In the PBS solution with GSH, the radii of NPs were 33.9 ± 14.0 , 83.4 ± 14.5 , 175.0 ± 47.9 , 328.0 ± 105.0 , and 575.0 ± 194.0 nm at 0, 2, 6, 12, and 24 hours, respectively (Figure 4(A)). The radii of STP-NPs were 33.3 ± 21.4 , 112.0 ± 17.2 , 188.0 ± 88.5 , 250.0 ± 64.9 , and 738.0 ± 303.0 nm at 0, 2, 6, 12, and 24 hours, respectively (Figure 4(A)). However, in PBS solutions without GSH, the radii of NPs or STP-NPs did not change significantly. The results indicated that under the stimulation of GSH, the particle sizes of NPs and STP-NPs increased. While in the absence of GSH, the diameter of these two kinds of nanoparticles was stable and maintained around 60.0 nm. There is a significant difference in GSH levels between tumor tissues and normal tissues *in vivo*. In general, the concentration of GSH is 1.0–2.0 $\mu\text{mol/L}$ in plasma, 2.0–20.0 $\mu\text{mol/L}$ in normal tissues, and 2.0–10.0 mmol/L in tumor cells (Schafer & Buettner, 2001). Based on this feature and the *in vitro* release test of our synthesized nanoparticles, we hypothesized that the

nanoparticles would exert a reduction-responsive ability to control drug release *in vivo*, thereby enhancing passive tumor targeting.

NPs and STP-NPs ($0\text{--}40.0 \text{ mg L}^{-1}$) were cultured with 143B osteosarcoma cells, and the biocompatibility of the nanoparticles was tested using MTT analysis. The nanoparticles had no toxic effect on osteosarcoma 143B cells. With increasing concentrations of NPs and STP-NPs, the viability of 143B osteosarcoma cells remained at high levels. It was reported that polyamino acids composed of less than two amino acids has good biocompatibility and weak immunogenicity (Gu et al., 2015). Therefore, phenylalanine and cystine were used as copolymers to fully ensure the biocompatibility of our synthesized nanoparticles.

NPs/DOX and STP-NPs/DOX were then constructed. The DLCs of NG/DOX and STP-NG/DOX were $8.95 \pm 0.07 \text{ wt.}\%$ and $9.82 \pm 0.14 \text{ wt.}\%$, respectively. The DLEs of NPs/DOX and STP-NPs/DOX were $29.45 \pm 1.42 \text{ wt.}\%$ and $29.70 \pm 2.03 \text{ wt.}\%$, respectively. Both of NPs/DOX and STP-NPs/DOX had high DLCs and DLEs, and the DLE did not decrease after the decoration of STP. Generally, DLC and DLE can be increased by enhancing the compatibility between the drug and the polymer. The drug encapsulation rate of the carrier mainly depends on the degree of hydrophobic interaction between the drug and the core of the polymer drug carrier. In this study, the amphiphilic polyamino acid can self-assemble in aqueous solution and the hydrophobic drug DOX can be

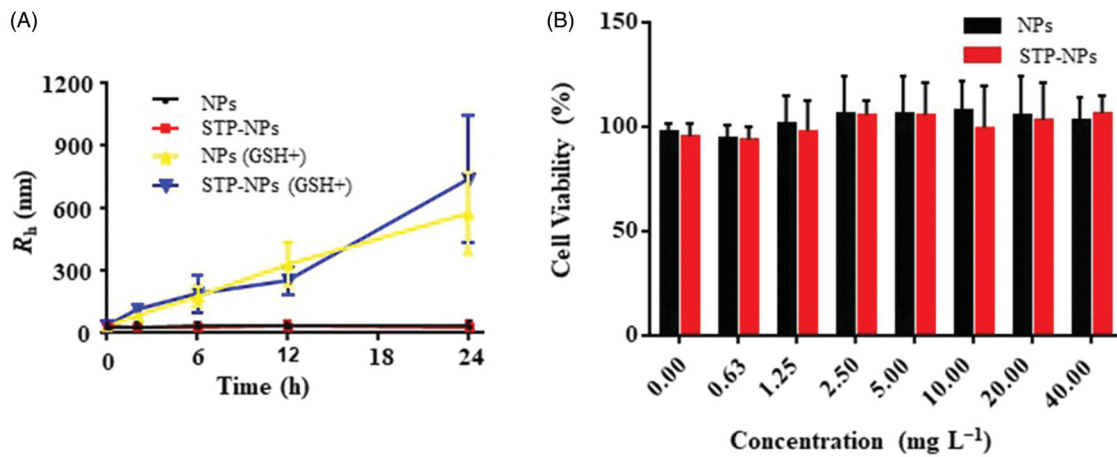


Figure 4. R_h changes of NPs and STP-NPs in GSH⁻ or GSH⁺ conditions (A) and *in vitro* cytotoxicities of NPs and STP-NPs toward 143B cells after incubation for 72 h (B).

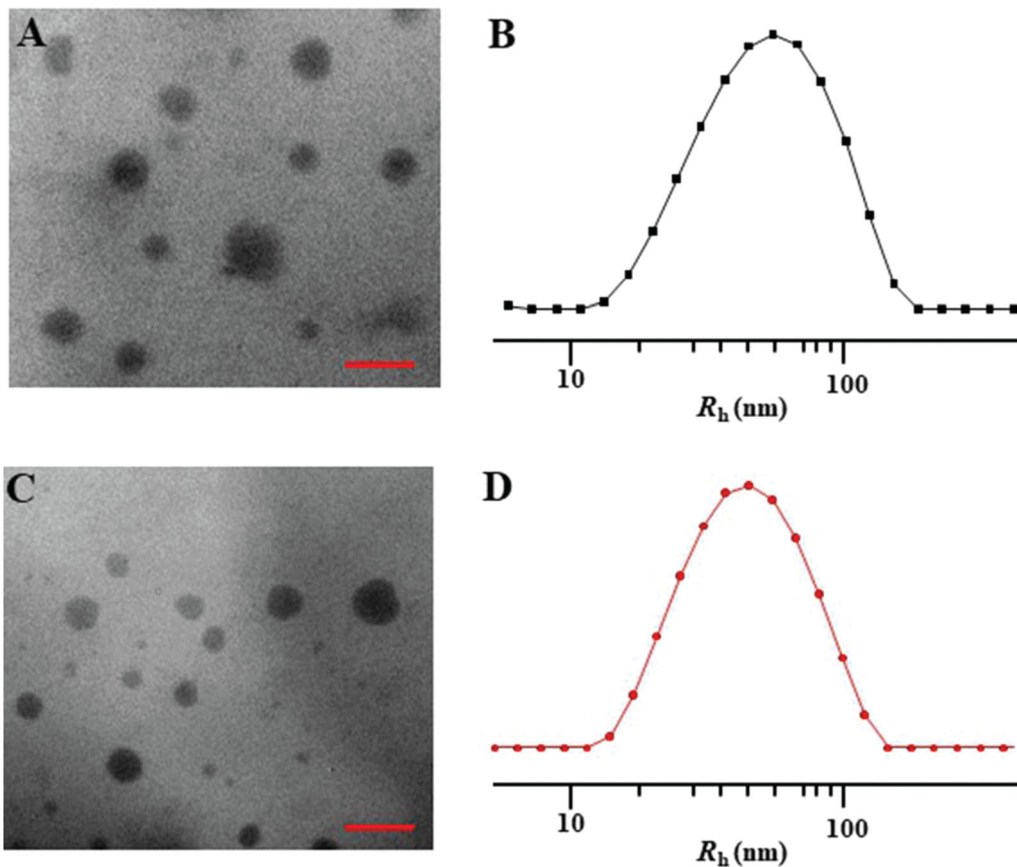


Figure 5. Typical TEM micrographs (A, C) and R_h s determined by DLS (B, D). NPs/DOX (A, B) and STP-NPs/DOX (C, D). Scale bar = 200 nm.

directly embedded in the hydrophobic core, which effectively improves the solubility and stability of the drug. In addition, the internal disulfide bonds increase the stability of the cross-linked core of the carrier. The structural characteristics of STP-NPs/DOX ensured the drug-carrying capacity and stability, enhanced the drug delivery ability, reduced the loss of DOX in the blood circulation, and ensured the therapeutic effect.

TEM analysis indicated that both NPs/DOX and STP-NPs/DOX were spherical, and the diameters of NPs/DOX and STP-NPs/DOX were 82.0 ± 21.0 nm and 69 ± 17.2 nm, respectively

(Figure 5(A,C)). In the DLS analysis, the diameters of NPs/DOX and STP-NPs/DOX were 124.8 ± 64.4 nm and 104.2 ± 52.8 nm, respectively (Figure 5(B,D)). The results showed that the diameter of the nanoparticles increased when DOX was incorporated. However, the size of the nanoparticles still within the optimal range (10–200 nm) required for a drug delivery system.

The release profiles of DOX from NPs/DOX and STP-NPs/DOX in PBS without or with 10.0 mM GSH are shown in Figure 6. The DOX release from NPs/DOX and STP-NPs/DOX reached equilibrium after 72 h. The release rates of DOX from

NPs/DOX in the GSH+ group and the GSH- group were 74.3% and 33.5%, respectively. The release rates of DOX from STP-NPs/DOX in the GSH+ group and GSH- group were 84.1% and 32.4%, respectively. For these two kinds of nanoparticles, there was a 41% and 52% difference in DOX release rates between the GSH+ group and GSH- group, respectively. The results demonstrated that DOX can be efficiently released from NPs/DOX and STP-NPs/DOX in PBS with 10.0 mM GSH. This is because that high levels of GSH can break the disulfide bonds, thus releasing DOX. Furthermore, compared with that of the F-DOX groups, we did not observe any obvious DOX burst release from the NPs/DOX or STP-NPs/DOX groups.

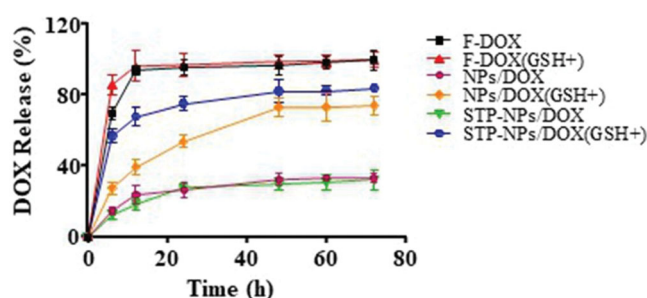


Figure 6. Release profiles of DOX from NPs/DOX and STP-NPs/DOX in PBS with or without 10.0 mM GSH.

CLSM and FCM were applied to analyze the *in vitro* uptake of DOX by 143B osteosarcoma cells and the release of DOX within cells. Compared with the GSH- group, the fluorescence intensity of DOX in the nuclei of the NPs/DOX and STP-NPs/DOX-treated cells both increased significantly in the GSH+ group (Figure 7). As a reducing substance, GSH is important to maintain the redox state in the tumor micro-environment. It can diffuse into the inner core of the nanoparticles and decompose the disulfide bond ($-SS-$) into two sulfhydryl groups ($-SH$) to accelerate the release of DOX (Wang et al., 2020b). Compared with NPs/DOX, the fluorescence intensity of DOX of in the STP-NPs/DOX-treated cells was higher in both GSH- and GSH+ groups. This is because vimentin is highly expressed on the surface of 143B osteosarcoma cells (Li et al., 2018c), and the targeted peptide-modified nanoparticles STP-NPs specifically binds to vimentin, which enhances the cell membrane's ability to transport DOX, thereby increasing the DOX concentration in the tumor cells. In the FCM analysis, compared with the GSH- group, the NPs-DOX and STP-NPs/DOX-treated cells in the GSH+ group had higher fluorescence intensities. Compared with the NPs/DOX-treated cells, the STP-NPs/DOX-treated cells in the GSH+ group and GSH- group had higher fluorescence intensity. These results were consistent with the results observed by CLSM.

MTT analysis was used to assess the *in vitro* suppression efficacies of F-DOX, NPs/DOX, and STP-NPs/DOX against 143B

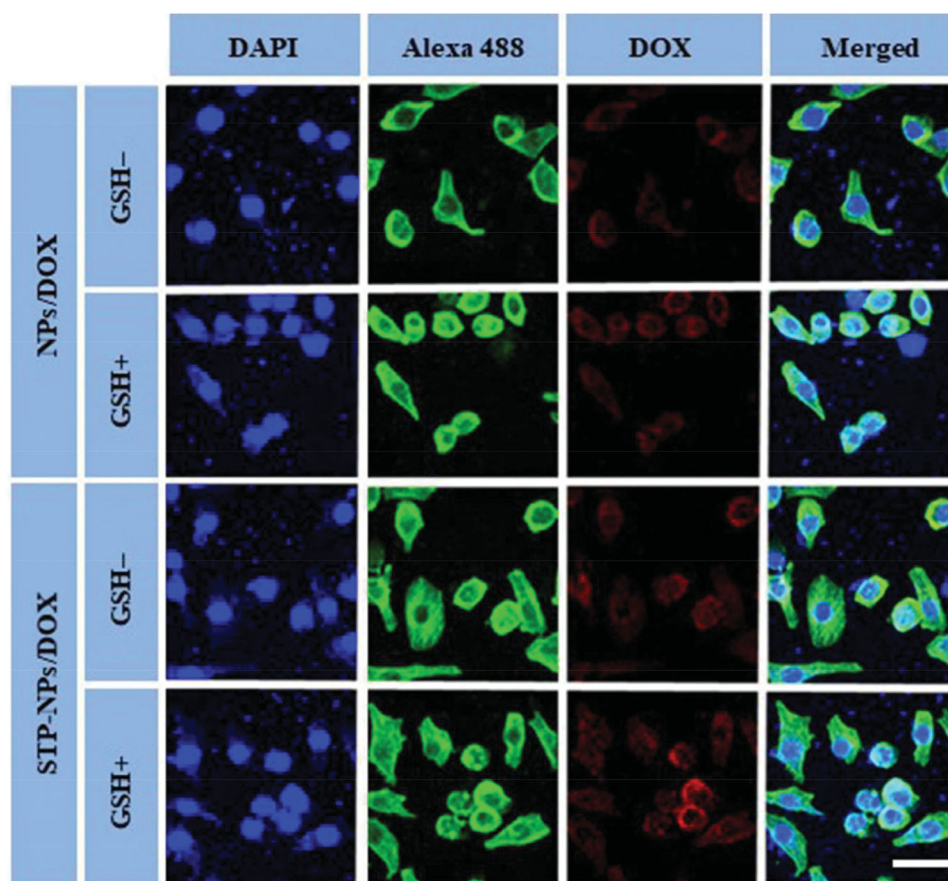


Figure 7. Typical CLSM images of NPs/DOX and STP-NPs/DOX intracellular uptake, with or without 10.0 mM GSH for two hours. From left to right, the images represent DAPI-stained cellular nuclei (blue), Alexa 488-stained F-actin (green), intracellular DOX fluorescence (red), and the overlays of above three images. Scale bar = 20 μ m.

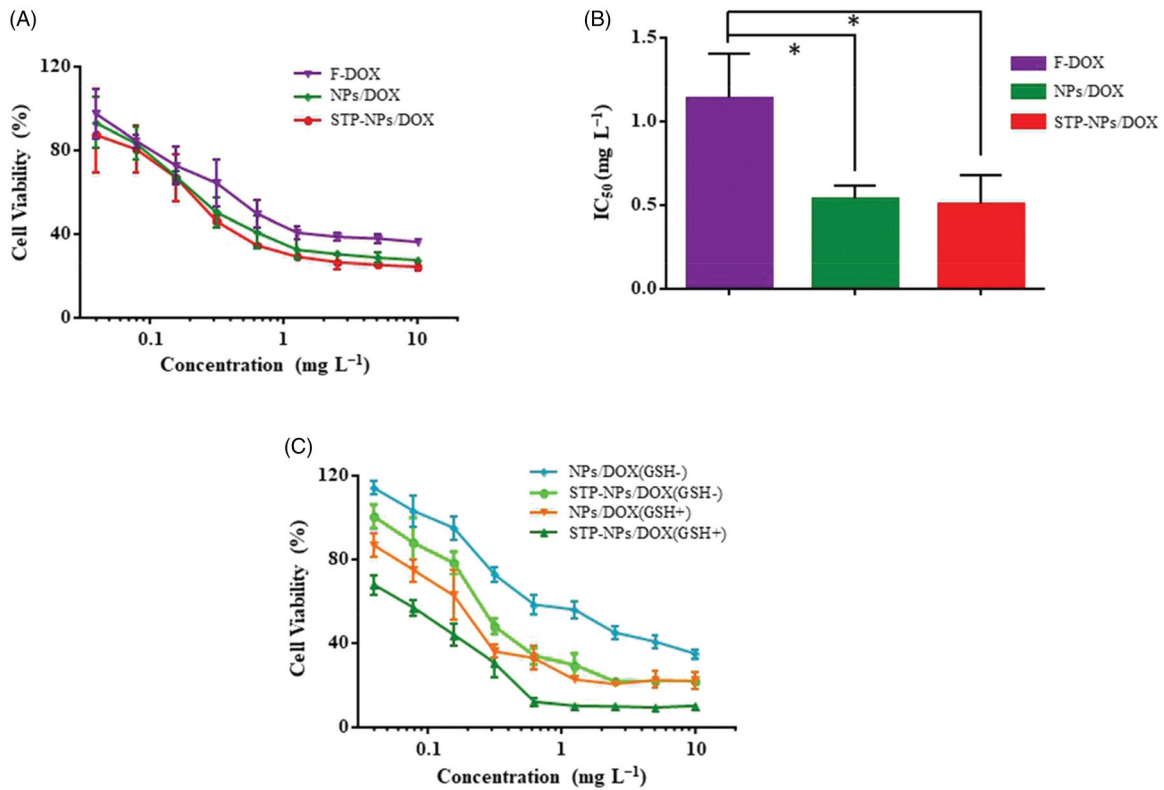


Figure 8. *In vitro* suppression efficacies of F-DOX, NPs/DOX, and STP-NPs/DOX against 143B osteosarcoma cells. (A) *In vitro* suppression efficacies of NPs/DOX and STP-NPs/DOX after incubation for 72 h. (B) IC₅₀ of F-DOX, NPs/DOX, and STP-NPs/DOX after 72 h ($n = 3$, $*p < .05$). (C) *In vitro* suppression efficacies of NPs/DOX and STP-NPs/DOX after incubation for 72 h, with or without 10.0 mM GSH for 2 h.

osteosarcoma cells. Compared with F-DOX, NPs/DOX, and STP-NPs/DOX could inhibit the proliferation of osteosarcoma cells more efficiently at different concentrations (Figure 8(A)). The 50% inhibitory concentration is shown in Figure 8(B). The IC₅₀s were $0.50 \pm 0.17 \text{ mg L}^{-1}$, $0.54 \pm 0.08 \text{ mg L}^{-1}$, and $1.15 \pm 0.26 \text{ mg L}^{-1}$ for the STP-NPs/DOX, NPs/DOX, and F-DOX groups, respectively. Compared with the F-DOX group, the IC₅₀ of the NPs/DOX and STP-NPs/DOX groups were lower ($*p < .05$). There were no significant differences in IC₅₀ between the NPs/DOX and STP-NPs/DOX groups, which indicated that at the same concentration, NPs/DOX and STP-NPs/DOX showed little difference in their abilities to inhibit the proliferation of 143B osteosarcoma cells *in vitro*. This is mainly because the *in vitro* experimental environment is completely different from the complex biological microenvironment *in vivo*, and many restrictions cannot fully reflect the metabolic process of the drug in the body. We co-cultured 143B cells for 72 hours with NPs/DOX and STP-NPs/DOX, with or without GSH pretreatment for two hours. Compared with the GSH⁻ group, NPs/DOX and STP-NPs/DOX in the GSH⁺ group showed more inhibitory effects on the proliferation of 143B cells.

Theoretically, nano-drug carriers can extend the time of drugs in blood circulation. In the animal study, we tested the pharmacokinetics of NPs/DOX, STP-NPs/DOX, and F-DOX. Compared with the free drug group, NPs/DOX and STP-NPs/DOX maintained higher plasma concentrations during the first 24 hours (Figure 9). The maximum concentration of F-DOX, NPs/DOX, and STP-NPs/DOX groups was 0.22, 1.53, and $1.16 \mu\text{g mL}^{-1}$, respectively. The average half-life ($T_{1/2}$) of DOX

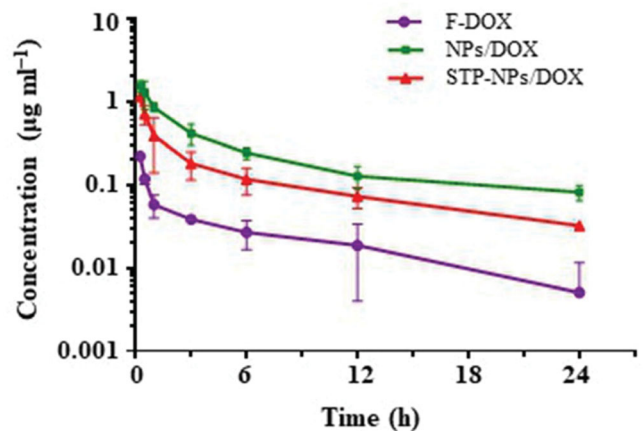


Figure 9. The pharmacokinetic of F-DOX, NPs/DOX, and STP-NPs/DOX.

in the NPs/DOX and STP-NPs/DOX groups was 9.77 and 12.12 hours, which were 1.34 and 1.66 times longer than that of F-DOX, respectively. These results indicated that the two reduction-sensitive NPs/DOX and STP-NPs/DOX have a good retention rate compared to F-DOX and can reduce the clearance rate and prolong the drug half-life time. Polyamino acids are a commonly used hydrophobic polymer material, which can achieve stable encapsulation of drugs. In our study, we further enhanced the hydrophilicity of the nanoparticle shell through PEGylation, which can reduce the adsorption of serum proteins during the blood circulation, prevent clearance via the reticuloendothelial system, and prolong the circulation time of the drug *in vivo* (Kolatte et al., 2014). The hydrophobic core seals DOX through physical

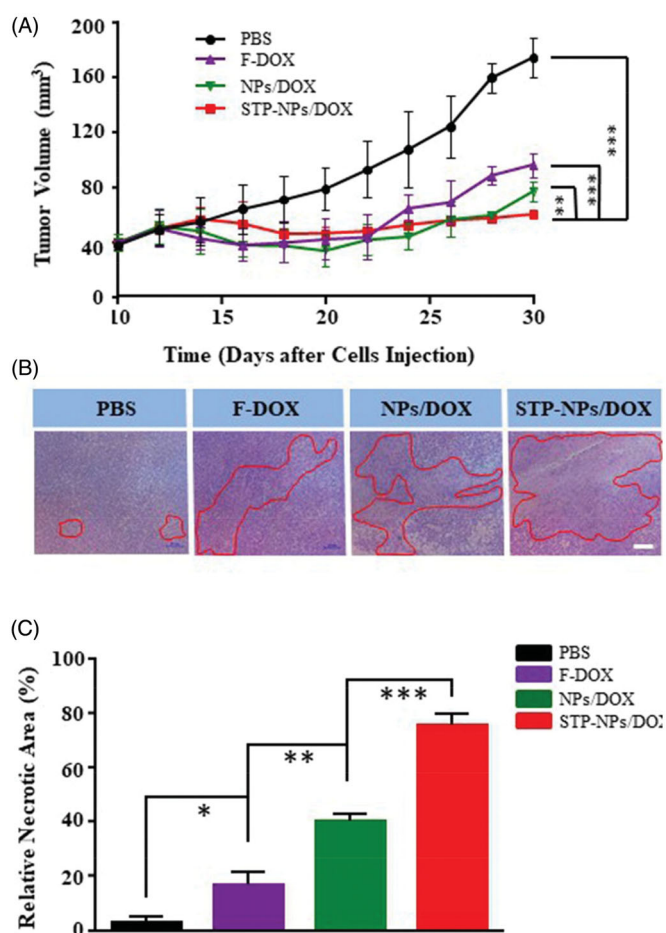


Figure 10. Anti-tumor efficacy of STP-NPs/DOX. (A) *In vivo* antitumor efficacies of F-DOX, NPs/DOX, and STP-NPs/DOX, with PBS as control ($n = 3$, $***p < 0.001$). (B) Histopathological analysis and (C) relative necrotic area of the tumor after treatment with PBS, F-DOX, NPs/DOX, and STP-NPs/DOX. Scale bar = $20 \mu\text{m}$ ($n = 3$, $*p < .05$, $**p < .01$, $***p < .001$). The red circles indicate the necrotic area of tumor tissues.

packaging, which improves the solubility and stability of the drug. Furthermore, the particle size of the nanoparticles is appropriate, which effectively reduces renal filtration and excretion, thereby maintaining a higher blood drug concentration. The long circulation of nanoparticles is conducive to reducing the systemic toxicity of DOX, and increasing DOX accumulation at tumor sites through the EPR effect, thereby achieving passive targeted delivery to tumor sites (Hayashi et al., 2009; Kolate et al., 2014).

The tumor inhibition efficiency of STP-NPs/DOX was evaluated in a 143B osteosarcoma mouse model. At the 30th day after the establishment of the mouse model, the tumor volume was $74.62 \pm 14.18 \text{ mm}^3$ in PBS group (Figure 10(A)). Compared with that in the PBS group, the tumor was significantly smaller in the other three groups ($***p < 0.001$). In addition, there was a statistically significant difference in tumor volume between the NPs/DOX and STP-NPs/DOX groups ($**p < 0.01$), which indicated that STP-NPs/DOX possessed the best tumor inhibition efficacy. H&E staining of tumor tissues and the relative necrotic area analysis were also used to further evaluate the tumor prevention effects of the different groups. In the PBS group, the tumor cells showed a regular spherical shape and the nucleus had obvious atypia (Figure

10(B)). However, in the F-DOX, NPs/DOX, and STP-NPs/DOX groups, a large amount of nuclear pyknosis or nuclear fragmentation was observed, and including the dissolution and disappearance of the nuclei. At the same time, extensive necrotic areas could be observed. The relative necrotic areas were $3.17 \pm 1.94\%$, $16.35 \pm 5.15\%$, $40.26 \pm 2.62\%$, and $75.26 \pm 4.28\%$ in PBS, F-DOX, NPs/DOX, and STP-NPs/DOX groups, respectively. The STP-NPs/DOX group had the largest relative necrotic area among the groups. In addition, there was a significant difference in the relative tumor necrosis area between the NPs/DOX and STP-NPs/DOX groups ($***p < .001$). Although passive targeting can benefit the drug accumulation at the tumor site, it cannot effectively deliver the drug to the deep tumor tissue. This is because compared with normal tissues, the osmotic pressure of the interstitial tissue in the tumor microenvironment is higher, which is not conducive for the nanocarriers to spread deeply. However, STP can positively bind with vimentin, which is highly expressed on the surface of osteosarcoma cells. As a result, the STP decorated nanoparticles possess an active tumor targeting ability. The passive and active tumor targeting ability of STP-NPs/DOX could result in the accumulation of DOX at the tumor site and deliver DOX to the deep tumor tissue, thus increasing DOX's tumor inhibition efficacy.

Immunofluorescence staining and semi-quantitative analysis of Ki-67 and caspase-3 were applied to evaluate the proliferation and necrosis of tumor cells in the different treatment groups (Figure 11). Consistent with the results of immunofluorescence staining, STP-NPs/DOX group showed the least amount of Ki-67, which indicated that STP-NPs/DOX could prevent the proliferation of osteosarcoma cells efficiently (Figure 11(A,C)). There was also a significant difference between the NPs/DOX and STP-NPs/DOX groups in the semi-quantitative analysis of Ki-67 ($**p < .01$). The STP-NPs/DOX group showed the highest caspase-3 levels among the groups (Figure 10(B,D)). This demonstrated that STP-NPs/DOX had a better tumor necrosis promotion effect than F-DOX and NPs/DOX. The passive and active targeting effects of STP-NPs/DOX resulted in efficient DOX delivery to tumor tissues and increased tumor inhibition efficacy.

The safety of anti-tumor drugs is important for further clinical application. In our study, H&E staining of major organs, body weight changes, and organ coefficients were used to evaluate the safety of STP-NPs/DOX. As a small molecular cytotoxic drug, the main mechanism of DOX is to inhibit DNA replication and RNA synthesis by activating topoisomerase II. However, this effect has no specific or special targets, and can easily cause systemic toxicity, especially cardiotoxicity. The toxic effect of DOX is dose-dependent. We have confirmed that the nanoparticles we synthesized have no toxic effect on 143B osteosarcoma cells. Thus, any toxicity caused by NPs/DOX and STP-NPs/DOX is mainly caused by DOX. In this study, we found that the synthesized nanoparticles could abrogate the toxic reaction caused by F-DOX. In the PBS group, there was no obvious tissue injuries in the heart, liver, spleen, lung, or kidney (Figure 12). Compared with those in the NPs/DOX and STP-NPs/DOX groups, there were obvious tissue damage to the heart, liver, lung, and

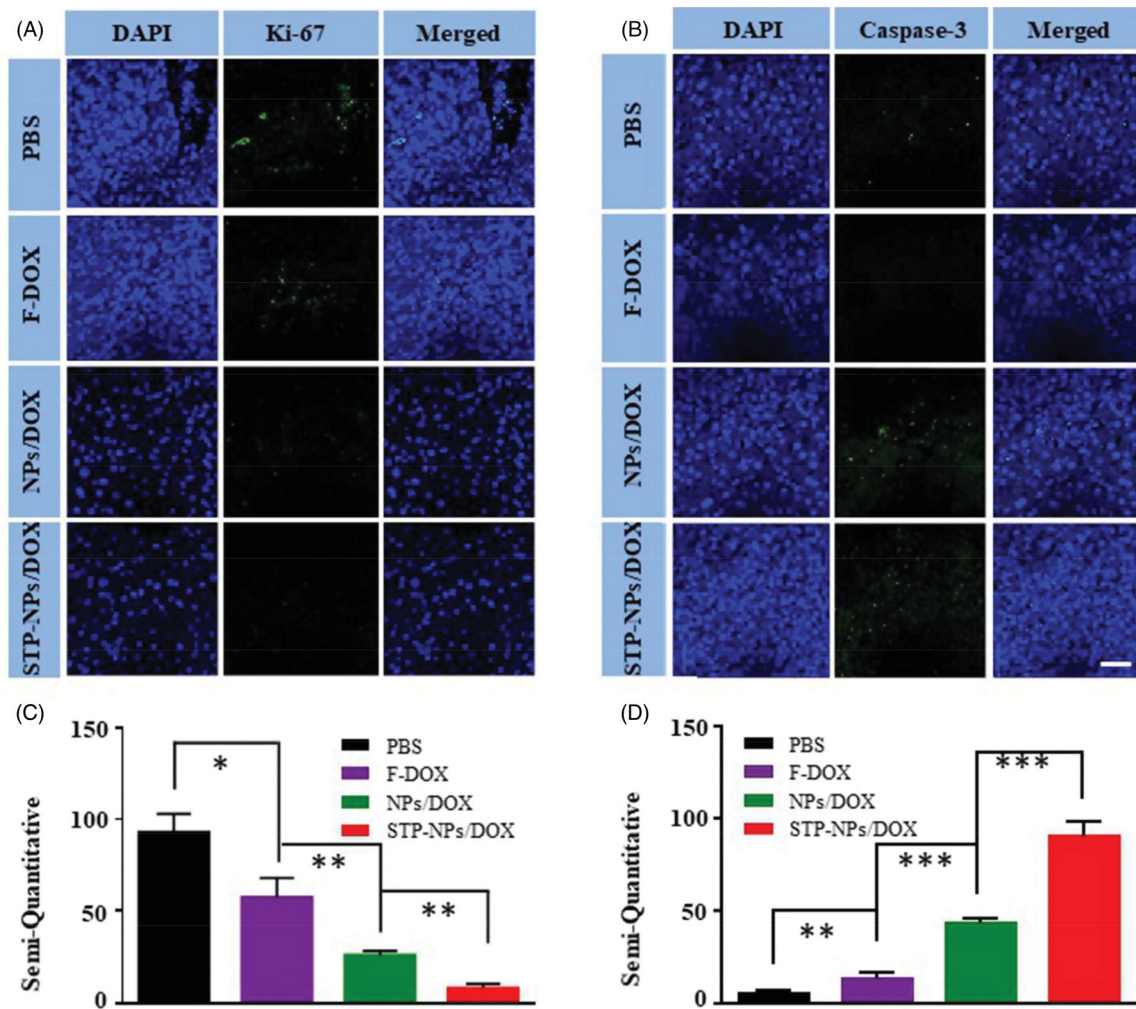


Figure 11. Immunofluorescence analysis of tumor tissues. (A, B) Immunofluorescence and (C, D) semi-quantitative results of (A, C) Ki-67 and (B, D) caspase-3 in the PBS, F-DOX, NPs/DOX, and STP-NPs/DOX groups ($n = 3$, $*p < .05$, $**p < .01$, $***p < .001$). Scale bar = 100 μm .

kidney in the F-DOX group. In detail, the degeneration and disordered arrangement of myocardial cells, and myocardial fiber breakage, could be observed. In liver tissues, hepatocytes were significantly shrunken and there was a large amount of inflammatory cell infiltration. In lung tissues, congestion, hyperplasia, and inflammatory cell infiltration were observed. In kidney, we found that some of the glomeruli had lost their normal shape. Compared with those in the F-DOX group, the above-mentioned pathological changes were milder in the NPs/DOX and STP-NPs/DOX groups, while the STP-NPs/DOX group showed the lowest level of organ damage, indicating that the peptide-modified nanoparticles have a stronger targeting effect when loaded with DOX to treat osteosarcoma, which indirectly reduces the side effects of DOX.

The body weight changes of mice and the organ coefficient were also applied to assess the safety of STP-NPs/DOX. The body weight of mice decreased gradually from the 10th day after the establishment of the osteosarcoma model in all groups. At the 30th day, the body weight of mice was the lowest in F-DOX group, while there was no difference between PBS and STP-NPs/DOX groups. However, the body weight was lower in the NPs/DOX group than that in the

STP-NPs/DOX group ($*p < .05$) (Figure 13(A)). The weight loss of animals is one of the important indicators to reflect drug toxicity. In the PBS group, as the weight of the mice decreased, there was a decrease in activity, and food and water intake. This was mainly caused by the massive diffusion of F-DOX within the body and the sharp increase in blood concentration, resulting in systemic toxicity. The weight of mice in the NPs/DOX and STP-NPs/DOX groups also decreased; however, the downward trend was eased, especially in the STP-NPs/DOX group, which showed the least weight loss. This may be attributed to the fact that DOX that is encapsulated within the nanoparticles in the NPs/DOX and STP-NPs/DOX groups can be slowly and continuously released, leading to accumulation in tumor tissues through active or passive targeting. As a result, the toxicity of DOX in the NPs/DOX and STP-NPs/DOX groups was small. The weight loss of mice in the PBS group was mainly caused by tumor-related cachexia.

Compared with those in the STP-NPs/DOX group, the organ coefficients of heart were lower in the PBS ($**p < .01$) and F-DOX ($*p < .05$) groups (Figure 13(B)). The organ coefficients of liver were lower in the NPs/DOX ($*p < .05$) and F-DOX ($*p < .05$) groups compared with that of the PBS group

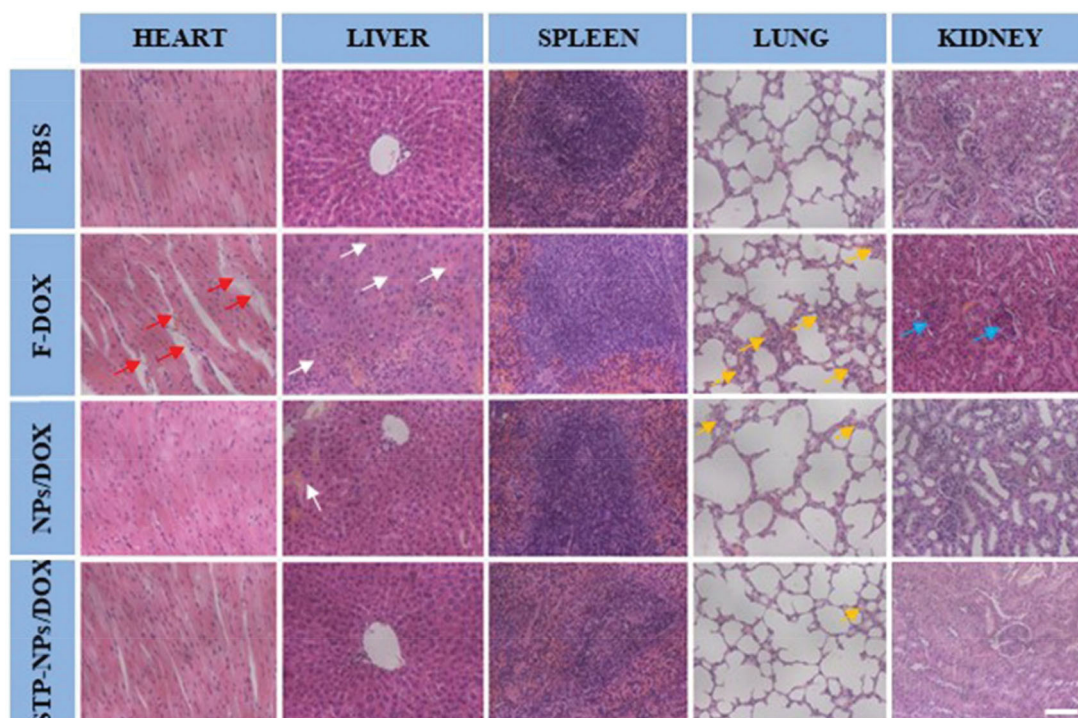


Figure 12. H&E staining of the heart, liver, spleen, lung, and kidney tissues from mice treated as indicated. Scale bar = 100 μ m. Red arrows indicate the breakage of myocardial fibers. White arrows indicate the shrunken hepatocytes and inflammatory cell infiltration in liver tissues. Yellow arrows indicate the congestion, hyperplasia, and inflammatory cell infiltration in lung tissues. Blue arrows indicate the abnormal glomeruli in kidney tissues.

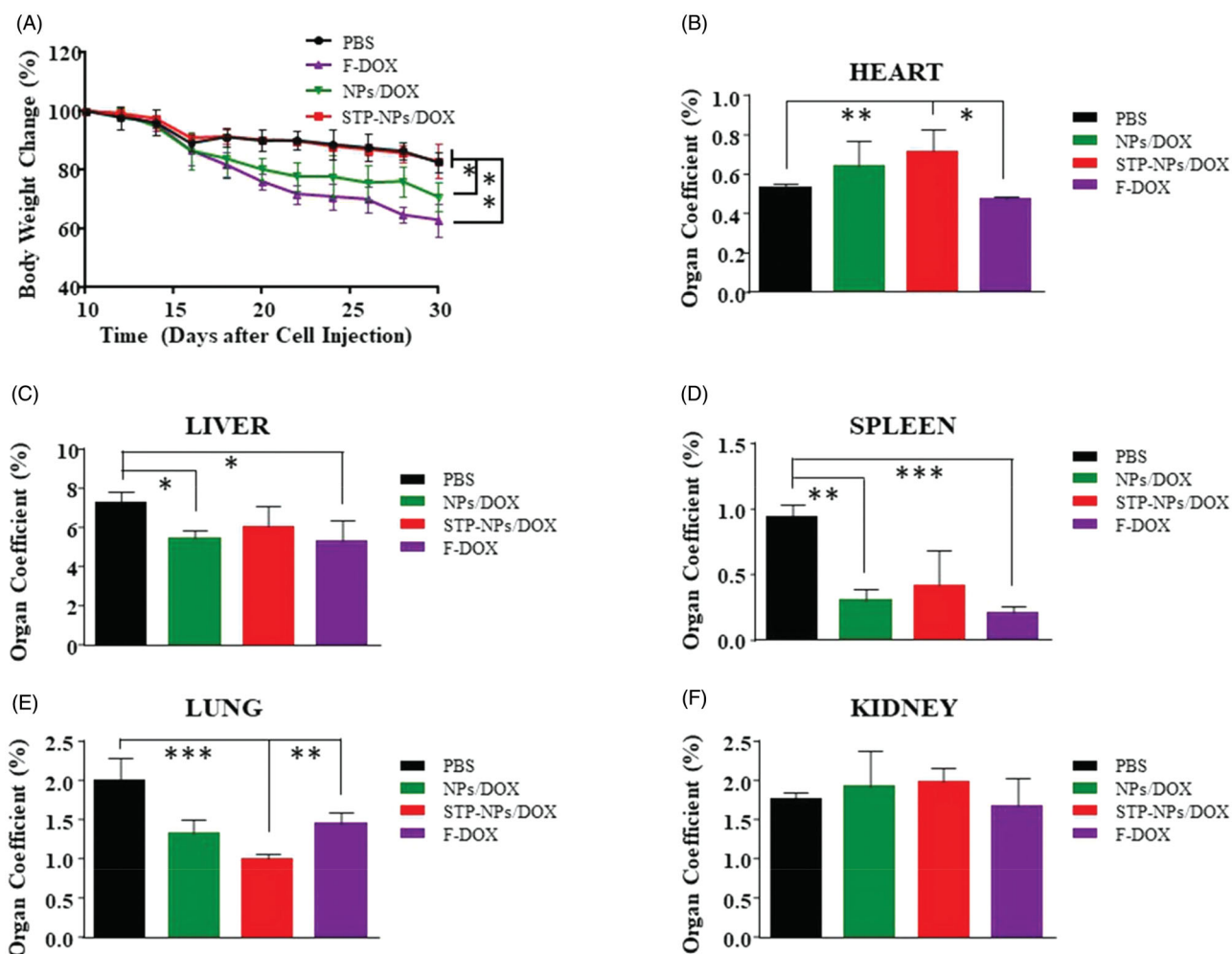


Figure 13. Body weight changes of mice and their organ coefficients. (A) Body weight changes of nude mice treated with PBS, F-DOX, NPs/DOX, and STP-NPs/DOX. The organ coefficients of (B) the heart, (C) the liver, (D) the spleen, (E) the lungs, and (F) the kidneys ($n = 3$, $*p < .05$, $**p < .01$, $***p < .001$).

(Figure 13(C)). Similar to the results for the liver, the organ coefficient in the spleen was higher in the PBS group than in the NPs/DOX group or F-DOX group (Figure 13(D)). There was also a significant difference in the organ coefficient of the lung between the STP-NPs/DOX and F-DOX groups (** $p < .01$). The organ coefficients of the heart, liver, and spleen of the F-DOX group mice decreased to varying degrees, while the organ coefficient of the lung was significantly higher than that of the STP-NPs/DOX group. The organ coefficients of the liver and spleen of the NPs/DOX group decreased. The organ coefficient study further confirmed the safety of STP-NPs/DOX.

Based on the above results, we found that the STP-NPs/DOX group had the lowest toxicity toward major organs, while the F-DOX group caused the most serious organ damage. The as synthesized nanoparticles could improve the controlled release of drugs, enhance the accumulation of drugs at tumor sites, significantly reduce the side effects caused by DOX, and improve the quality of life of tumor-bearing mice. These results effectively promote the application of our designed nanocarriers loaded with DOX in osteosarcoma chemotherapy.

Conclusions

In the present study, STP decorated mPEG-P(Phe-co-Cys) nanoparticles was successfully developed through amino acid ring-opening polymerization. The synthesized copolymers with polyamino acids can self-assemble in aqueous solution to form spherical nanoparticles, with a suitable particle size, good biocompatibility, safety and stability, and a good controllable drug release ability. NPs and STP-NPs possess internal disulfide bonds, and can load DOX through encapsulation. NPs/DOX and STP-NPs/DOX can achieve reduction-responsive drug release in the osteosarcoma microenvironment, which extends the blood circulation time and increases the uptake of DOX within tumor tissues. In particular, STP-NPs/DOX possess both passive and active tumor targeting effects, which are more effective for DOX accumulation at tumor sites and for controlled drug release. STP-NPs/DOX not only increases the tumor inhibition efficiency against osteosarcoma, but also reduces the side effects of DOX toward major organs.

Disclosure statement

The authors report no conflict of interest.

Author contributions

RQ: Investigation, Methodology, and Formal analysis. DS: Investigation, Methodology, and Formal analysis. YB: Investigation, Methodology, and Formal analysis. RQ and DS: Formal analysis and Writing - review & editing. JL and LW: Conceptualization and Writing - review & editing.

Funding

This work was supported by the Department of Finance of Jilin Province (3D5197434429) and National Natural Science Foundation of China (3A4205367429).

References

- Botter SM, Neri D, Fuchs B. (2014). Recent advances in osteosarcoma. *Curr Opin Pharmacol* 16:15–23.
- Chen L, Zhao L, Hu G, et al. (2020). Tumor-specific nanomedicine via sequential catalytic reactions for accurate tumor therapy. *J Mater Chem B* 8:6857–65.
- Choi HS, Liu W, Misra P, et al. (2007). Renal clearance of quantum dots. *Nat Biotechnol* 25:1165–70.
- Eaton BR, Schwarz R, Vatner R, et al. (2020). Osteosarcoma. *Pediatr Blood Cancer* e28352.
- Feng X, Li J, Zhang X, et al. (2019). Electrospun polymer micro/nanofibers as pharmaceutical repositories for healthcare. *J Control Release* 302:19–41.
- Gu X, Ding J, Zhang Z, et al. (2015). Polymeric nanocarriers for drug delivery in osteosarcoma treatment. *Curr Pharm Des* 21:5187–97.
- Harrison DJ, Geller DS, Gill JD, et al. (2018). Current and future therapeutic approaches for osteosarcoma. *Expert Rev Anticancer Ther* 18:39–50.
- Hayashi K, Zhao M, Yamauchi K, et al. (2009). Systemic targeting of primary bone tumor and lung metastasis of high-grade osteosarcoma in nude mice with a tumor-selective strain of *Salmonella typhimurium*. *Cell Cycle* 8:870–5.
- Kolata A, Baradia D, Patil S, et al. (2014). PEG – a versatile conjugating ligand for drugs and drug delivery systems. *J Control Release* 192:67–81.
- Li J, Xu W, Chen J, et al. (2018a). Highly bioadhesive polymer membrane continuously releases cytostatic and anti-inflammatory drugs for peritoneal adhesion prevention. *ACS Biomater Sci Eng* 4:2026–36.
- Li J, Xu W, Li D, et al. (2018b). Locally deployable nanofiber patch for sequential drug delivery in treatment of primary and advanced orthotopic hepatomas. *ACS Nano* 12:6685–99.
- Li S, Zhang T, Xu W, et al. (2018c). Sarcoma-targeting peptide-decorated polypeptide nanogel intracellularly delivers shikonin for upregulated osteosarcoma necroptosis and diminished pulmonary metastasis. *Theranostics* 8:1361–75.
- Ma L, Xu Y, Xu X. (2020). Targeted MEK inhibition by cobimetinib enhances doxorubicin's efficacy in osteosarcoma models. *Biochem Biophys Res Commun* 529:622–8.
- Maeda H, Nakamura H, Fang J. (2013). The EPR effect for macromolecular drug delivery to solid tumors: improvement of tumor uptake, lowering of systemic toxicity, and distinct tumor imaging in vivo. *Adv Drug Deliv Rev* 65:71–9.
- Marina N, Gebhardt M, Teot L, Gorlick R. (2004). Biology and therapeutic advances for pediatric osteosarcoma. *Oncologist* 9:422–41.
- Qiu S, Tao L, Zhu Y. (2019). Marital status and survival in osteosarcoma patients: an analysis of the surveillance, epidemiology, and end results (SEER) database. *Med Sci Monit* 25:8190–203.
- Ren X, Su C. (2020). Sphingosine kinase 1 contributes to doxorubicin resistance and glycolysis in osteosarcoma. *Mol Med Rep* 22:2183–90.
- Schafer FQ, Buettner GR. (2001). Redox environment of the cell as viewed through the redox state of the glutathione disulfide/glutathione couple. *Free Radic Biol Med* 30:1191–212.
- Strouhalova K, Prechová M, Gandalovičová A, et al. (2020). Vimentin intermediate filaments as potential target for cancer treatment. *Cancers* 12:184.
- Su T, Yang B, Gao T, et al. (2020). Polymer nanoparticle-assisted chemotherapy of pancreatic cancer. *Ther Adv Med Oncol* 12:1758835920915978.

- Torchilin V. (2011). Tumor delivery of macromolecular drugs based on the EPR effect. *Adv Drug Deliv Rev* 63:131–5.
- Torchilin VP. (2007). Targeted pharmaceutical nanocarriers for cancer therapy and imaging. *AAPS J* 9:E128–E47.
- Wakhloo NT, Anders S, Badique F, et al. (2020). Actomyosin, vimentin and LINC complex pull on osteosarcoma nuclei to deform on micro-pillar topography. *Biomaterials* 234:119746.
- Wang J, Byrne JD, Napier ME, Desimone JM. (2011). More effective nanomedicines through particle design. *Small* 7:1919–31.
- Wang X, Ding X, Yu B, et al. (2020a). Tumor microenvironment-responsive polymer with chlorin e6 to interface hollow mesoporous silica nanoparticles-loaded oxygen supply factor for boosted photodynamic therapy. *Nanotechnology* 31:305709.
- Wang X, Yang L, Fang Q, et al. (2020b). GLUT1-targeting and GSH-responsive DOX/L61 nanodrug particles for enhancing MDR breast cancer therapy. *Part Part Syst Charact* 37:2000165.
- Yang B, Chen Y, Shi J. (2020). Tumor-specific chemotherapy by nanomedicine-enabled differential stress sensitization. *Angew Chem Int Ed Engl* 59:9693–701.
- Yu Z, Xiao Z, Shuai X, Tian J. (2020). Local delivery of sunitinib and Ce6 via redox-responsive zwitterionic hydrogels effectively prevents osteosarcoma recurrence. *J Mater Chem B* 8:6418–28.